

## Soliton supermode transitions and total red shift suppression in multi-core fibers

A. ANTIKAINEN<sup>1,\*</sup>  AND G. P. AGRAWAL<sup>1,2</sup> 

<sup>1</sup>The Institute of Optics, University of Rochester, Rochester, New York 14627, USA

<sup>2</sup>Laboratory for Laser Energetics, 250 East River Rd, Rochester, New York 14623, USA

\*Corresponding author: aku.antikainen@rochester.edu

Received 6 May 2019; revised 17 July 2019; accepted 20 July 2019; posted 22 July 2019 (Doc. ID 366760); published 22 August 2019

**Soliton propagation in seven-core fibers is studied numerically with the frequency dependence of linear coupling taken into account. It is shown that under certain conditions, solitons can undergo spontaneous supermode transitions upon abrupt red shift, analogous to the recently discovered phenomenon of soliton self-mode conversion in step-index multi-mode fibers. When the core separation is increased, the dynamics change drastically, leading to total suppression of soliton self-frequency shift and the emergence of spatially oscillating solitonic structures with resemblance to solitons in graded-index multi-mode fibers. The observed phenomena are general multi-core effects and not specific to seven-core fibers.** © 2019 Optical Society of America

<https://doi.org/10.1364/OL.44.004159>

The simplest example of a multi-core fiber is given by a fiber coupler in which two cores are in close proximity separated by a distance of the same order of magnitude as the core diameter. Optical nonlinearities in such couplers were first exploited for intensity-dependent transmission characteristics [1,2], and an analytical and numerical study of solitons in such couplers was subsequently conducted [3]. Three-core couplers were shown to have some advantages over two-core couplers [4], and the  $N$ -core linear array case has been studied from the discrete self-focusing point of view [5].

Recent interest in space division multiplexing has put multi-core fibers back in the spotlight, owing to their potential applications in optical communication systems [6]. Linear coupling between the cores mitigates detrimental nonlinearities [7,8], and, notably, a coupled-core fiber can outperform single-mode fibers with the same design parameters, as has been shown for four-core fibers [9]. More recently, the same was demonstrated for a seven-core fiber [10], indicating that multi-core fibers could in general offer increased transmission capacity compared to their single-mode fiber bundle counterparts. Multi-core fibers have also found applications in pulse compression and pulse combining [11] as well as high average power supercontinuum generation [12].

In this Letter, we numerically investigate propagation of solitons in a seven-core fiber where the cores are all identical and arranged in a regular hexagonal pattern. The refractive index

$n_{\text{clad}}(\lambda)$  of the cladding has been computed from the Sellmeier equation for silica [13], and the core index is taken to be  $n_{\text{core}}(\lambda) = n_{\text{clad}}(\lambda) + 0.01$  across the whole spectrum. The core radius is 3  $\mu\text{m}$ , and the core separation is varied. To model light propagation in such fibers, we use the coupled-core version of the generalized nonlinear Schrödinger equation [14]:

$$\begin{aligned} \frac{\partial \tilde{A}_p(z, \omega)}{\partial z} = & i[\beta(\omega) - \beta_0 - \beta_1(\omega - \omega_0)]\tilde{A}_p(z, \omega) \\ & + i\gamma(\omega)\mathcal{F}\{[R(t) * |A_p(z, t)|^2]A_p(z, t)\}(\omega) \\ & + i\sum_{l \neq p} \kappa_{pl}(\omega)\tilde{A}_l(z, \omega), \end{aligned} \quad (1)$$

where  $A_p(z, t)$  is the temporal envelope of the field in the  $p$ th core at the carrier frequency  $\omega_0 = 2\pi c/\lambda_0$  with  $\lambda_0 = 1.55 \mu\text{m}$ , and  $\tilde{A}_p(z, \omega)$  is its Fourier transform defined as

$$\tilde{A}_p(z, \omega) = \mathcal{F}\{A_p(z, t)\}(\omega) = \int_{-\infty}^{\infty} A_p(z, t)e^{i\omega t} dt. \quad (2)$$

The expression in the square brackets in Eq. (1) accounts for dispersion, and the frequency-dependent propagation constant  $\beta(\omega)$  has been computed by solving the full characteristic equation without the weak guidance assumption for a step-index fiber that each of the cores represents. In other words,  $\beta(\omega)$  is the propagation constant of the fundamental mode in an isolated core in an infinite cladding. The subtraction of the terms  $\beta_0 = \beta(\omega_0)$  and  $\beta_1 = [d\beta/d\omega]_{\omega=\omega_0}$  inside the square brackets means that the equation has been written in the frame of reference where the group velocity of the input pulse centered at 1.55  $\mu\text{m}$  is zero.  $R(t) = (1 - f_R)\delta(t) + f_R b_R(t)$  is the nonlinear response function that includes the Kerr and Raman effects with a Raman fraction of  $f_R = 0.18$ . The Raman response function in the frequency domain,  $H_R(\omega)$ , is modeled after the experimental Raman data for fused silica [15]. The nonlinear parameter  $\gamma(\omega) = n_2\omega/[cA_{\text{eff}}(\omega)]$  is determined by using  $n_2 = 3.2 \cdot 10^{-20} \text{ m}^2/\text{W}$  and computing the fundamental mode effective area for each frequency in an isolated core. For the center frequency, we have  $\gamma(\omega_0) = 3.27 \text{ (kmW)}^{-1}$ . Note that inter-core nonlinear interactions have not been included in Eq. (1), but we have also verified that their omission has a negligible effect on the simulation results. The linear coupling coefficients  $\kappa_{pl}(\omega)$  are

frequency-dependent and are calculated using the formula derived in Ref. [16]. Linear coupling is considered only between nearest neighbors such that the center core is coupled to all other six cores, and each core in the periphery is coupled to the center core and its other two neighbors. The coupling coefficient  $\kappa_{pl}(\omega)$  between cores  $p$  and  $l$  is therefore either zero (if cores  $p$  and  $l$  are not neighbors) or some positive function of  $\omega$ , which will from now on be denoted by simply  $\kappa(\omega)$ .

In the absence of nonlinearities ( $\gamma = 0$ ), Eq. (1) has single-frequency solutions that propagate in the seven-core fiber without changing their transverse field profiles with only the phase changing linearly with propagation distance  $z$ . These patterns are called supermodes of the fiber, and assuming the associated fields can be expressed as linear combinations of the fields in the individual cores [17], their fields are of the form  $\tilde{\mathbf{A}}(z, \omega) = \tilde{\mathbf{F}}(\omega)e^{i\beta^s(\omega)z}$ , where  $\tilde{\mathbf{A}}(z, \omega) = [\tilde{A}_1(z, \omega), \dots, \tilde{A}_7(z, \omega)]^T$  is a vector of the core fields (in some chosen order),  $\tilde{\mathbf{F}}(\omega)$  is a vector independent of  $z$ , and  $\beta^s(\omega)$  is the propagation constant of the supermode. Using this ansatz in Eq. (1) with  $\gamma = 0$  then leads to the matrix equation

$$i\beta^s(\omega)\tilde{\mathbf{F}}(\omega) = i\beta(\omega)\tilde{\mathbf{F}}(\omega) - i\mathbf{K}(\omega)\tilde{\mathbf{F}}(\omega), \quad (3)$$

where  $\mathbf{K}(\omega)$  is the coupling matrix, and the equation has been written in the laboratory frame of reference. The equation can be rewritten as

$$[(\beta - \beta^s)\mathbf{I} - \mathbf{K}]\tilde{\mathbf{F}} = \mathbf{0}. \quad (4)$$

The non-trivial solutions of Eq. (4) correspond to the coefficient matrix  $(\beta - \beta^s)\mathbf{I} - \mathbf{K}$  having a zero determinant, and the supermode propagation constants can be determined from this condition. The analytical solutions for the propagation constants of the supermodes of a seven-core fiber are then

$$\begin{aligned} \beta^A(\omega) &= \beta(\omega) + (1 + \sqrt{7})\kappa(\omega), \\ \beta^B(\omega) &= \beta(\omega) + \kappa(\omega), \\ \beta^C(\omega) &= \beta(\omega) - \kappa(\omega), \\ \beta^D(\omega) &= \beta(\omega) + (1 - \sqrt{7})\kappa(\omega), \\ \beta^E(\omega) &= \beta(\omega) - 2\kappa(\omega), \end{aligned} \quad (5)$$

where the superscripts denote different supermodes. Modes  $B$  and  $C$  are two-fold degenerate, bringing the total number of supermodes to seven.  $A$  and  $D$  are the only ones with six-fold symmetry, with  $D$  having a higher concentration of energy in the center core compared to  $A$ . Using the center core as the input core thus initially divides the energy unevenly between  $A$  (31.1%) and  $D$  (68.9%), with no energy in the other supermodes.

The input field launched in the center core is of the form  $A(0, t) = \sqrt{P_0} \text{sech}(t/T_0)$  with quantum shot noise included as one photon per frequency bin. The input pulse duration (full width at half maximum) is fixed at 100 fs, meaning  $T_0 \approx 56.73$  fs, and the peak power  $P_0$  is varied between 1611.65 W (corresponding to a fundamental soliton for a single core) and 20 kW. Figure 1 shows the temporal and spectral evolution when the input field with  $P_0 = 10$  kW is launched into the center core in a fiber where the center-to-center separation between neighboring cores is 16  $\mu\text{m}$ . Since the input is launched into the center core, the fields in all outer cores will (under ideal conditions) be identical, and it suffices to show the evolution in the center core and one outer core.

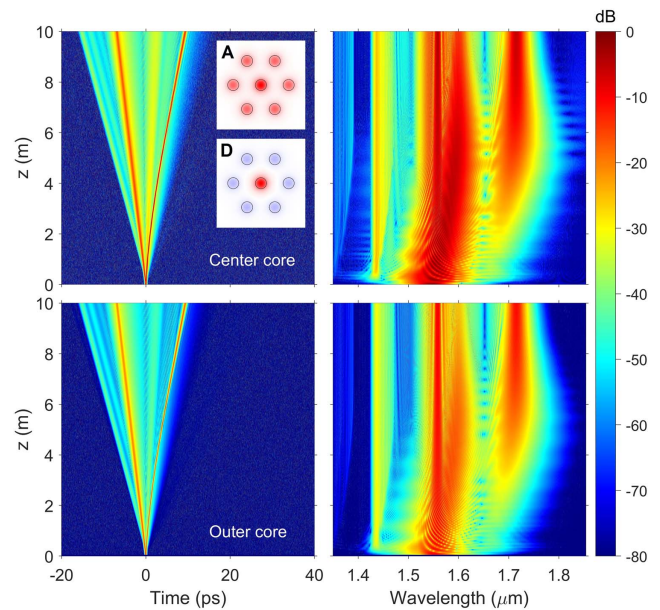


**Fig. 1.** Temporal (left column) and spectral (right column) evolution of a 10 kW input pulse launched in the center core of a seven-core fiber with the core centers separated by 16  $\mu\text{m}$ . The top row corresponds to the center core and the bottom row to an outer core. The color scale is in dB normalized to the corresponding temporal or spectral total intensity in all cores. The insets show the field distributions of the participating supermodes  $A$  and  $D$  with red corresponding to positive electric field and blue to negative.

Due to the different propagation constants of the two excited supermodes  $A$  and  $D$ , the pulse splits into two daughter pulses that become separated in time. In terms of phase velocity, supermode  $D$  is faster than supermode  $A$ , but the opposite is true for their group velocities, and the trailing daughter pulse is in supermode  $D$ . Both daughter pulses become solitons, but the leading pulse takes a longer distance to become one, since it needs to increase its duration to compensate for its smaller peak power and energy. The amplitude of the trailing pulse is larger, and therefore the resulting soliton is shorter in duration and starts to experience soliton self-frequency shift (SSFS).

Besides the SSFS of the trailing soliton, there are two other remarkable features in the spectra in Fig. 1: the generation of blue-shifted spectral components with wavelengths shorter than 1.5  $\mu\text{m}$ , and the somewhat abrupt-looking red shift of the soliton from 1.6  $\mu\text{m}$  to 1.72  $\mu\text{m}$ , leaving a gap in the spectrum around 1.65  $\mu\text{m}$ . The generation of the blue-shifted components is due to temporal reflections [18]. The solitons cause temporally varying refractive index barriers through cross-phase modulation, and the remaining pump components reflect off these moving barriers changing their frequency upon reflection [19]. Only the trailing pulse in Fig. 1 is intense enough to slow down because of nonlinearities and cause the paths of the pulse and the pump remnants to cross to enable temporal reflections (see Visualization 1). Whereas the blue-shifted components are due to temporal reflections, the sudden jump in the red shift looks exactly like the recently discovered multi-mode fiber phenomenon of soliton self-mode conversion [20,21].

To understand why the abrupt red shift occurs, we need to use the supermode picture. The soliton field in the core is

initially out of phase with the fields in the outer cores by  $\pi$  radians (a characteristic of supermode  $D$ ), but after the abrupt red shift, the fields in all cores are in phase (a characteristic of  $A$ ). The soliton therefore switches from supermode  $D$  to  $A$  during the discontinuous shift. The continuity and smoothness of the temporal trajectory of the trailing soliton in Fig. 1 indicates that the group velocity of the pulse does not abruptly change upon the supermode transition. Figure 2 shows the group velocities of different supermodes for the fiber used in Fig. 1 together with color-coded Raman gain showing which wavelengths would experience Raman gain from a pump with a matching group velocity in supermode  $D$ .

The fact that the group velocity curve of supermode  $A$  falls exactly on the Raman gain peak for a wide wavelength range in Fig. 2 means that a pulse in supermode  $D$  will copropagate with a pulse in  $A$  provided that the central frequency of the pulse in  $A$  is smaller by approximately 13.2 THz, which is the peak of Raman gain in silica. The trailing soliton initially in supermode  $D$  will therefore transfer energy to the emerging copropagating soliton in  $A$  through Raman scattering, which manifests as the discontinuous red shift and makes this phenomenon the multi-core equivalent of soliton self-mode conversion. The same supermode transition observations were made for all input powers, but the distance at which the power transfer between supermodes  $A$  and  $D$  takes place decreasing with increasing pump power.

Equation (5) shows how the supermode propagation constants depend on the coupling  $\kappa(\omega)$  between neighboring cores. Increasing the separation between the cores decreases the coupling between them and therefore the supermode propagation constants converge toward that of an isolated core. For large core separations, no two pulses in different supermodes can be group velocity matched for frequency separations close to the peak of the Raman gain. It is therefore to be expected that Raman-induced power transfer between supermodes cannot be observed for large core separations. Figure 3 shows the evolution of the same 10 kW input pulse launched into the center core of a fiber where the cores are separated by 25  $\mu\text{m}$ .

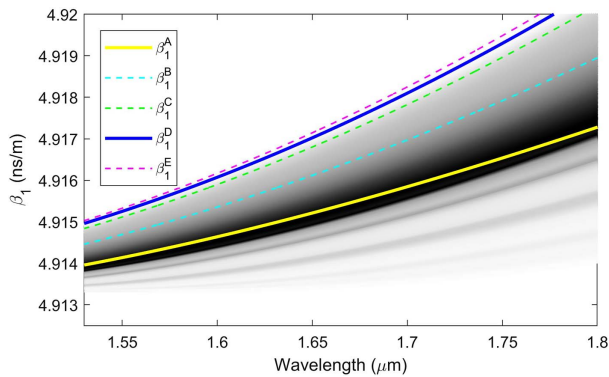


**Fig. 2.** Inverse of group velocity ( $\beta_1$ ) of the supermodes of a seven-core fiber with 16  $\mu\text{m}$  core separation. The thick solid lines correspond to the supermodes that are excited by pumping the center core and the dashed lines to the ones that lack six-fold symmetry. The shaded background indicates Raman gain from a group velocity matched pump in supermode  $D$  with white denoting no gain and black denoting maximal gain. The frequency separation (measured in the horizontal direction) from the  $\beta_1^D$  curve to the (black) peak of the Raman gain is thus always 13.2 THz.

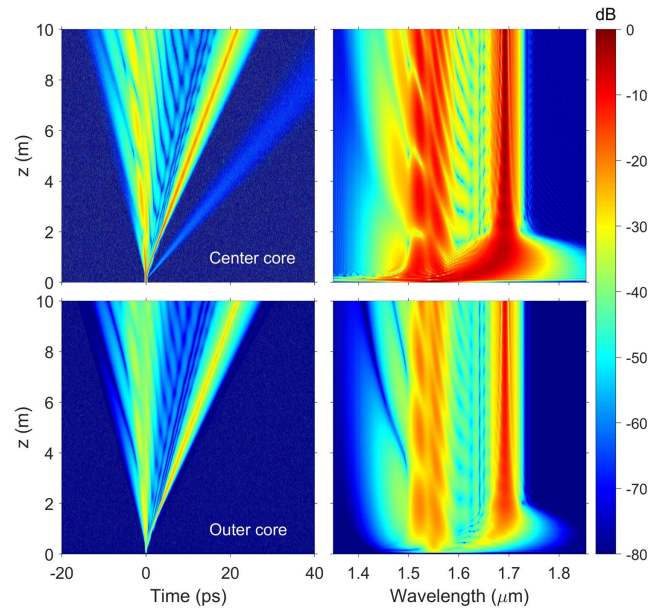


**Fig. 3.** Same as Fig. 1 but with a 25  $\mu\text{m}$  center-to-center core separation. (Also see Visualization 2.)

Again, the pulse splits into two main pulses separated in time within the first 50 cm of propagation. The trailing part forms a soliton while the leading daughter pulse disperses and spreads its intensity over time upon propagation. However, this time the pulse splitting cannot be attributed to the different group velocities of supermodes  $A$  and  $D$ , as the rate of daughter pulse separation due to the group velocity difference is only 38 fs/m. No pulse splitting was observed for a 25  $\mu\text{m}$  core separation in the absence of nonlinearities. The splitting in Fig. 3 is therefore caused by optical nonlinearities. The intense soliton forming in Fig. 3 experiences a smaller group velocity because of the Kerr effect and further decelerates due to the Raman-induced SSFS [22]. The SSFS is initially very rapid, and the soliton shifts to approximately 1.69  $\mu\text{m}$  from the initial center wavelength of 1.55  $\mu\text{m}$  within the first two meters of propagation. The rapid red shift is explained by the fact that initially the forming soliton is short, only 45 fs in duration (FWHM), and the rate of red shift is proportional to  $T_{\text{FWHM}}^{-4}$ . The coupling length is  $1/\kappa = 1.77$  m at 1.55  $\mu\text{m}$ , which means that little power is transferred from the center core to the outer cores during the initial stages of propagation. The soliton essentially propagates as it would in an isolated core for approximately one meter. Then soon after, something drastic happens, and suddenly the SSFS stops completely. To understand why the SSFS is suppressed, it is informative to look at the wavelength dependence of the coupling coefficient  $\kappa(\omega)$  and the nonlinearity  $\gamma(\omega)$ , as shown in Fig. 4.

The increase in  $\kappa(\omega)$  with wavelength means that the soliton that was initially mostly confined in the center core is transferring energy to the outer cores at an accelerating rate as the soliton red shifts.  $\kappa(\lambda)$  increases from the initial  $\kappa(1.55 \mu\text{m}) = 0.566 \text{ m}^{-1}$  to  $\kappa(1.69 \mu\text{m}) = 2.02 \text{ m}^{-1}$ , and the energy of the soliton redistributes among the cores. The soliton perceives this as effective loss, which in turn is accompanied by an increase in duration from 45 fs to 540 fs and naturally hinders SSFS. Even though  $\gamma$  decreases with wavelength, by turning the

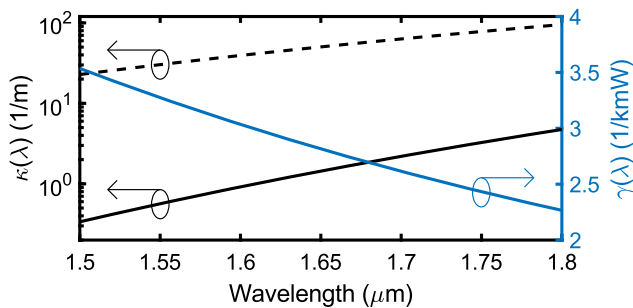


**Fig. 4.** Coupling coefficient  $\kappa$  (left scale, solid black line) for a fiber with 25  $\mu\text{m}$  core separation. The dashed line corresponds to a core separation of 16  $\mu\text{m}$  and is shown for comparison. The nonlinearity parameter  $\gamma$  (right scale) is independent of core separation.

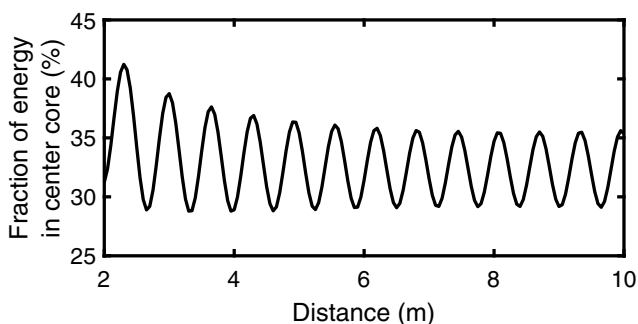


**Fig. 5.** Fraction of trailing pulse energy in the center core as a function of propagation distance.

frequency dependence of  $\gamma$  and  $\kappa$  off in the simulations one at a time, we found that linear coupling and the associated spatial redistribution of energy were solely responsible for hindering SSFS. Using  $\kappa(\lambda) = \kappa(1.55 \mu\text{m})$  showed no SSFS suppression, while  $\kappa(\lambda) = \kappa(1.69 \mu\text{m})$  yielded results similar to Fig. 3. This means that  $\kappa$  should be treated as wavelength-dependent in multi-core simulations, as its omission can yield unphysical results.

After the SSFS has stopped, the trailing pulse propagates in a stable manner but with periodic oscillations in the energy distribution among the cores. These oscillations are illustrated in Fig. 5, which shows the fraction of pulse energy in the center core. After the transient stage, the energy in the center core oscillates between 29% and 36% of the total soliton energy with an oscillation period of 64 cm. This indicates that the pulse, though mostly in supermode  $A$ , is not completely pure in terms of supermodes, but instead a dynamic combination of  $A$  and  $D$ . Pulses in multi-core fibers can thus undergo a periodic form of discrete self-focusing and experience spatial oscillations similar to those of solitons in graded-index multi-mode fibers [23]. After the spectral compression stage, the pulse also develops temporal wings that gradually spread in time on both sides of the main pulse, but nevertheless the pulse maintains many soliton-like properties and is held together by an interplay of nonlinearities, coupling, and dispersion.

In conclusion, we have numerically studied soliton propagation in seven-core step-index fibers and demonstrated that solitons can undergo supermode transitions upon abrupt red shift if the participating supermodes are group velocity matched

for a frequency separation close to the silica Raman gain peak at 13.2 THz. Such transitions were recognized as the multi-core analog of soliton self-mode conversion in step-index multi-mode fibers. We also showed that in the weak coupling regime, such transitions cannot occur, as the supermodes can be group velocity matched only for small frequency separations, but the weak coupling regime supports other phenomena of interest. Namely, we observed total soliton self-frequency shift suppression due to frequency-dependent linear coupling, and spatially oscillating solitonic structures similar to multi-mode solitons in graded-index multi-mode fibers. Depending on the coupling regime, step-index multi-core fibers can therefore display behavior similar to both step-index and graded-index multi-mode fibers as well as support phenomena unobserved in either.

**Funding.** National Science Foundation (ECCS-1505636).

**Acknowledgment.** The authors acknowledge William A. Wood, Petr Sterlingov, and John D. Downie of Corning Inc. for helpful discussions.

## REFERENCES

1. S. M. Jensen, *IEEE J. Quantum Electron.* **18**, 1580 (1982).
2. A. M. Maier, *Kvantovaya Elektron. (Moscow)* **9**, 2296 (1982), *Sov. J. Quantum Electron.* **12**, 1490 (1982).
3. N. Akhmediev and A. Ankiewicz, *Phys. Rev. Lett.* **70**, 2395 (1993).
4. N. Finlayson and G. I. Stegeman, *Appl. Phys. Lett.* **56**, 2276 (1990).
5. D. N. Christodoulides and R. I. Joseph, *Opt. Lett.* **13**, 794 (1988).
6. T. Hayashi, Y. Tamura, T. Hasegawa, and T. Taru, *J. Lightwave Technol.* **35**, 450 (2017).
7. S. Mumtaz, R.-J. Essiambre, and G. P. Agrawal, *IEEE Photon. Technol. Lett.* **24**, 1574 (2012).
8. C. Antonelli, O. Golani, M. Shtaf, and A. Mecozzi, *Opt. Express* **25**, 13055 (2017).
9. R. Ryf, N. K. Fontaine, S. H. Chang, J. C. Alvarado, B. Huang, J. Antonio-López, H. Chen, R.-J. Essiambre, E. Burrows, R. W. Tkach, R. Amezcua-Correa, T. Hayashi, Y. Tamura, T. Hasegawa, and T. Taru, in *European Conference on Optical Communication (ECOC)* (2017), paper M.2.E.1.
10. R. Ryf, J. C. Alvarado-Zacarias, S. Wittek, N. K. Fontaine, R. Essiambre, H. Chen, R. Amezcua-Correa, H. Sakuma, T. Hayashi, and T. Hasegawa, in *Optical Fiber Communications Conference and Exhibition (OFC)* (Optical Society of America, 2019), paper Th4B.3.
11. A. M. Rubenchik, L. S. Chekhovskoy, M. P. Fedoruk, O. V. Shtyrina, and S. K. Turitsyn, *Opt. Lett.* **40**, 721 (2015).
12. H. F. Wei, H. W. Chen, S. P. Chen, P. G. Yan, T. Liu, L. Guo, Y. Lei, Z. L. Chen, J. Li, X. B. Zhang, G. L. Zhang, J. Hou, W. J. Tong, J. Luo, J. Y. Li, and K. K. Chen, *Laser Phys. Lett.* **10**, 045101 (2013).
13. I. H. Malitson, *J. Opt. Soc. Am.* **55**, 1205 (1965).
14. G. P. Agrawal, *Nonlinear Fiber Optics*, 5th ed. (Academic, 2013).
15. R. H. Stolen, J. P. Gordon, W. J. Tomlinson, and H. A. Haus, *J. Opt. Soc. Am. B* **6**, 1159 (1989).
16. R. Tewari and K. Thyagarajan, *J. Lightwave Technol.* **4**, 386 (1986).
17. G. P. Agrawal, *Lightwave Technology: Components and Devices* (Wiley, 2004).
18. B. W. Plansinis, W. R. Donaldson, and G. P. Agrawal, *Phys. Rev. Lett.* **115**, 183901 (2015).
19. A. Antikainen, F. R. Arteaga-Sierra, and G. P. Agrawal, *Phys. Rev. A* **95**, 033813 (2017).
20. A. Antikainen, L. Rishøj, B. Tai, S. Ramachandran, and G. P. Agrawal, *Phys. Rev. Lett.* **122**, 023901 (2019).
21. L. Rishøj, B. Tai, P. Kristensen, and S. Ramachandran, *Optica* **6**, 304 (2019).
22. F. M. Mitschke and L. F. Mollenauer, *Opt. Lett.* **11**, 659 (1986).
23. W. H. Renninger and F. W. Wise, *Nat. Commun.* **4**, 1719 (2013).